Progress In Electromagnetics Research B, Vol. 32, 129–147, 2011

THEORETICAL AND EXPERIMENTAL EVALUATION OF SUPERSTRATE EFFECT ON RECTANGULAR PATCH RESONATOR PARAMETERS

N. Aouabdia[1, *], N. E. Belhadj-Tahar[1], G. Alquie[1], and F. Benabdelaziz[2]

[1]Laboratoire d'Electronique et d'Electromagnétisme (L2E), UPMC Paris 06, F-75005 Paris, France

[2]Laboratoire de Microsystème et Instrumentation, Université Mentouri Constantine, Campus Ahmed Hamani, Route Ain El Bey, 25000 Constantine, Algerie

Abstract—In this paper, modeling and experimentation of a Rectangular Patch Resonator (RPR) covered with a dielectric superstrate are investigated. The RPR criteria are established theoretically and experimentally, to be used in future prospects as an electromagnetic (EM) sensor for the characterization of superstrates. The theoretical model is based on the moment method (MoM) via Galerkin's approach, in which three types of basis and testing functions are used. These functions as well as the spectral dyadic Green function are efficiently implanted with compact structured Fortran 90 codes. The EM commercial HFSS and CST Microwave Studio softwares are used to simulate the proposed RPR prototypes. The accuracy of the obtained results is assessed using four prototypes of RPRs operating around 6 GHz, taking into account only the resonant frequency of the fundamental dominant mode. The theoretical model is compared to simulation and measurement results, and very good agreements are observed.

1. INTRODUCTION

Over the last two decades, microwave resonators have become an important subject of interest. They are used in a variety of applications, including sensors, filters, oscillators, frequency meters and tuned amplifier [1]. Resonator elements based on microstrip

Received 26 May 2011, Accepted 2 July 2011, Scheduled 11 July 2011

* Corresponding author: Nabila Aouabdia (nabila.aouabdia@etu.upmc.fr).

technology are conformable and have minimized shape, low weight and cost. Hence, they are commonly used in many commercial applications in the industry, such as mobile satellite communications or direct broadcast satellite services, but also as nondestructive testing sensors for material evaluation.

Patch resonator performances, such as resonant frequency and quality factor, are dependent on the dielectric parameters of different materials involved in their structures. In microwave system applications, dielectrics for substrate and superstrate are realized with very low losses materials to obtain the best performances. When used as sensors, some of the dielectric layers can be constituted with unknown material; the changes in the resonator parameters, mainly frequency shift and increase of the quality factor, are related to the complex permittivity of this unknown material. In this particular application, a patch sensor may be used to assess permittivity of particular layers by comparing between patch measured parameters with a reference structure and those obtained with the unknown material. Accuracy of structures modeling and measurements data is necessary to obtain, by solving the inverse problem, obtaining good values of the dielectric parameters of the unknown material, or highlighting local variations of the dielectric permittivity.

This paper is focused on the exhaustive comparison among a theoretical modeling of a Rectangular Patch Resonator (RPR), electromagnetic simulations with commercial software's and measurements of selected structures. RPRs have been studied extensively using rigorous full-wave analysis and various types of current expansion functions [2–4]. The proposed theoretical analysis is based on the Method of Moment (MoM) which is considered as a standard procedure to solve problems [5–8] such as the fundamental quantity of interest, namely the electric current distribution on the patch surface, from which all the other required resonator parameters can be obtained [2–9]. In the literature, three types of entire domain basis functions are widely used to expand the patch currents. While, the first two types of basis functions involve a set of sinusoidal cavity modes without edge conditions (sbf-wo-ec) [9, 10] and with edge conditions (sbf-w-ec) [10], and in order to incorporate the edge conditions (cp-ec), the third one consists of Chebyshev polynomials combinations with weighting factors [11]. The accuracy of these theoretical results has been compared with electromagnetic simulations using HFSS and CST softwares and with previous published works.

Four RPR prototypes have been realized with different substrate thicknesses, with and without superstrate. In order to quantify the effects of the results dispersion due to the real physical dimensions

of the resonators, all their dimensions have been carefully measured. These values have been introduced for comparison in the EM simulators as a new set of parameters. This procedure gives an estimation of the variation of the results due to geometrical dimensions of the resonators.

2. THEORETICAL MODEL

2.1. Geometrical Structure

The proposed prototype is shown in Figure 1. The RPR whose dimensions are (a, b) along the two axis (ox, oy), respectively, is printed on a grounded uniaxial dielectric slab of thickness d_1.

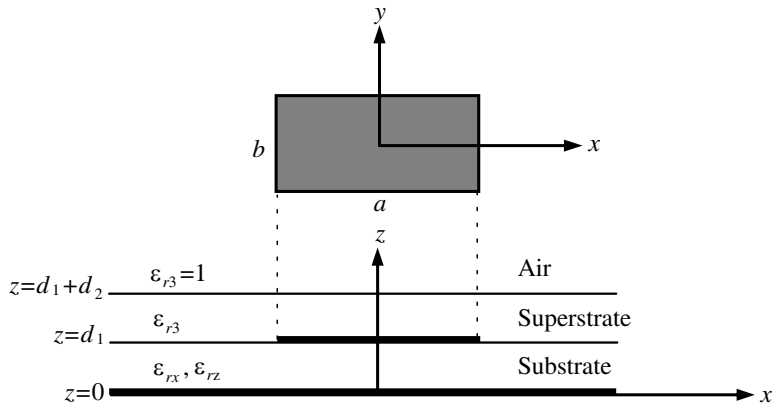

Figure 1. Geometrical structure of the rectangular patch loaded with superstrate on uniaxial substrate.

The permittivity tensor in this region is given by

$$\bar{\varepsilon} = \varepsilon_0 \text{diag}\left[\varepsilon_{rx}, \varepsilon_{rx}, \varepsilon_{rz}\right] \tag{1}$$

A non-magnetic dielectric material with permeability μ_0 covers the entire resonant patch, as a superstrate layer of thickness d_2 and relative permittivity ε_{r2}.

2.2. Theory

Starting from Maxwell's equations with limit conditions at the interfaces applied to this structure, a grounded uniaxial substrate covered with an isotropic superstrate, we first determine the closed form of the spectral Green's dyad at $z = d_1$ [12–14]

$$\bar{\mathbf{G}}(\mathbf{k}_s) = \frac{1}{i\omega\varepsilon_0}\mathrm{diag}\left[\frac{N^e}{D^e}k_z^e, \frac{N^h}{D^h}k_0^2\right]\cdot\sin(\bar{\mathbf{k}}_z d_1) \tag{2}$$

where, N^e, N^h, D^e and D^h are defined as follows

$$\begin{aligned}
N^e &= k_z\cos(k_{2z}d_2) + i\frac{k_{2z}}{\varepsilon_2}\sin(k_{2z}d_2)\\
N^h &= \cos(k_{2z}d_2) + i\frac{k_z}{k_{2z}}\sin(k_{2z}d_2)\\
D^e &= \cos(k_{2z}d_2)\left[\varepsilon_x k_z\cos(k_z^e d_1) + ik_z^e\sin(k_z^e d_1)\right]\\
&\quad + i\sin(k_{2z}d_2)\left[\frac{\varepsilon_x}{\varepsilon_2}k_{2z}\cos(k_z^e d_1) + i\varepsilon_2\frac{k_z k_z^e}{k_{2z}}\sin(k_z^e d_1)\right]\\
D^h &= \cos(k_{2z}d_2)\left[k_z^h\cos(k_z^h d_1) + ik_z\sin(k_z^h d_1)\right]\\
&\quad + i\sin(k_{2z}d_2)\left[\frac{k_z k_z^h}{k_{2z}}\cos(k_z^h d_1) + ik_{2z}\sin(k_z^h d_1)\right]\\
k_z^e &= \left(\varepsilon_x k_0^2 - \frac{\varepsilon_x}{\varepsilon_z}k_s^2\right)^{1/2}, \quad k_z^h = \left(\varepsilon_x k_0^2 - k_s^2\right)^{1/2}, \quad k_0^e = \omega^2\mu_0\varepsilon_0,\\
k_{2z} &= \left(\varepsilon_2 k_0^2 - k_s^2\right)^{1/2} \quad \text{and} \quad k_z = \left(k_0^2 - k_s^2\right)^{1/2}
\end{aligned}$$

$k_s = \hat{x}k_x + \hat{y}k_y$ is called the transverse wave vector.

Since the total tangential electric field due to the surface current $\mathbf{J}$ vanishes on the microstrip patch [12–14], the following integral equation may be obtained

$$\int_{-\infty}^{\infty}\int d\mathbf{k}_s\bar{\mathbf{F}}(\mathbf{k}_s,\mathbf{r}_s)\cdot\bar{\mathbf{G}}(\mathbf{k}_s)\cdot\tilde{\mathbf{J}}(\mathbf{k}_s) = 0 \tag{3a}$$

where, $\bar{\mathbf{F}}(\mathbf{k}_s,\mathbf{r}_s)$ is the kernel of the vector Fourier transforms and is given by

$$\bar{\mathbf{F}}\left(\mathbf{k}_s,\mathbf{r}_s\right) = \frac{1}{k_s}\begin{bmatrix} k_x & k_y \\ k_y & -k_x \end{bmatrix} e^{i\mathbf{k}_s\cdot\mathbf{r}_s} \tag{3b}$$

where, $\mathbf{r}_s = x\hat{\mathbf{x}} + y\hat{\mathbf{y}}$ and $k_s = |\mathbf{k}_s|$.

As usual, in order to solve the integral Equation (3a), we use the Galerkin MoM in the Fourier transform domain. The surface current $\mathbf{J}$

on the patch is then expanded into finite series of known basis functions J_{xn} and J_{ym} as

$$\mathbf{J}(\mathbf{r_s}) = \sum_{n=1}^{N} a_n \begin{bmatrix} J_{xn}(\mathbf{r_s}) \\ 0 \end{bmatrix} + \sum_{m=1}^{M} b_m \begin{bmatrix} 0 \\ Jym(\mathbf{r_s}) \end{bmatrix} \tag{4}$$

where, a_n and b_m are the mode expansion coefficients. Therefore, the integral Equation (3a) can be written as a linear set of equations leading to the following set of matrix equation given by (5a)

$$\begin{bmatrix} \left(\bar{\mathbf{B}}_1\right)_{N\times N} & \left(\bar{\mathbf{B}}_2\right)_{N\times M} \\ \left(\bar{\mathbf{B}}_3\right)_{M\times N} & \left(\bar{\mathbf{B}}_4\right)_{M\times M} \end{bmatrix} \cdot \begin{bmatrix} (\mathbf{a})_{N\times 1} \\ (\mathbf{b})_{M\times 1} \end{bmatrix} = 0 \tag{5a}$$

where,

$$\left(\bar{\mathbf{B}}_1\right)_{kn} = \int_{-\infty}^{+\infty}\int d\mathbf{k_s} \frac{1}{k_s^2}\left[k_x^2 G^e + k_y^2 G^h\right] \tilde{J}_{xk}(-\mathbf{k_s})\tilde{J}_{xn}(\mathbf{k_s}) \tag{5b}$$

$$\left(\bar{\mathbf{B}}_2\right)_{km} = \int_{-\infty}^{+\infty}\int d\mathbf{k_s} \frac{k_x k_y}{k_s^2}\left[G^e - G^h\right] \tilde{J}_{xk}(-\mathbf{k_s})\tilde{J}_{ym}(\mathbf{k_s}) \tag{5c}$$

$$\left(\bar{\mathbf{B}}_3\right)_{\ln} = \int_{-\infty}^{+\infty}\int d\mathbf{k_s} \frac{k_x \cdot k_y}{k_s^2}\left[G^e - G^h\right] \tilde{J}_{yl}(-\mathbf{k_s})\tilde{J}_{xn}(\mathbf{k_s}) \tag{5d}$$

$$\left(\bar{\mathbf{B}}_4\right)_{lm} = \int_{-\infty}^{+\infty}\int d\mathbf{k_s} \frac{1}{k_s^2}\left[k_x^2 G^e + k_y^2 G^h\right] \tilde{J}_{yl}(-\mathbf{k_s})\tilde{J}_{ym}(\mathbf{k_s}) \tag{5e}$$

For a non-trivial solution of (5a), we must have

$$\det\left(\bar{\mathbf{B}}\right) = 0 \tag{6}$$

The condition given by (6) is the characteristic equation of the complex resonant frequency $f = f_r + if_{im}$. The quality factor and half power bandwidth are defined by

$$Q = f_r/2f_{im} \tag{7}$$

$$BW = 1/Q \tag{8}$$

2.3. Basis Functions

To study the convergence of the method, we have chosen three types of basis functions developed in the subsequent subsections [3].

2.3.1. Sinusoidal Basis Functions without Edge Conditions (sbf-wo-ec)

The set of the entire-domain sinusoidal basis functions without edge conditions is given by Newman and Forraï as

$$\mathbf{J}_{xn}(\mathbf{r_s}) = \sin\left[\frac{n_1\pi}{a}\left(x+\frac{a}{2}\right)\right]\cdot\cos\left[\frac{n_2\pi}{b}\left(y+\frac{b}{2}\right)\right] \tag{9}$$

$$\mathbf{J}_{ym}(\mathbf{r_s}) = \cos\left[\frac{m_1\pi}{a}\left(x+\frac{a}{2}\right)\right]\cdot\sin\left[\frac{m_2\pi}{b}\left(y+\frac{b}{2}\right)\right] \tag{10}$$

where, n_1, n_2, m_1 and m_2 are positive integers. The scalar Fourier transforms of (9) and (10) are given by Equations (11) and (12), respectively

$$\tilde{\mathbf{J}}_{xn}(\mathbf{k_s}) = \tilde{I}_{xn}\cdot\tilde{I}_{xm} \tag{11}$$

$$\tilde{\mathbf{J}}_{ym}(\mathbf{k_s}) = \tilde{I}_{yn}\cdot\tilde{I}_{ym} \tag{12}$$

where,

$$\tilde{I}_{xn}=\frac{ia}{2}\left[e^{-i\frac{n_1\pi}{2}}\cdot\sin c\left[(k_{n_1}+k_x)\frac{a}{2}\right]-e^{i\frac{n_1\pi}{2}}\cdot\sin c\left[(k_{n_1}-k_x)\frac{a}{2}\right]\right] \tag{13}$$

$$\tilde{I}_{xm}=\frac{b}{2}\left[e^{-i\frac{n_2\pi}{2}}\cdot\sin c\left[(k_{n_2}+k_y)\frac{b}{2}\right]+e^{i\frac{n_2\pi}{2}}\cdot\sin c\left[(k_{n_2}-k_y)\frac{b}{2}\right]\right] \tag{14}$$

$$\tilde{I}_{yn}=\frac{a}{2}\left[e^{-i\frac{m_1\pi}{2}}\cdot\sin c\left[(k_{m_1}+k_x)\frac{a}{2}\right]+e^{i\frac{m_1\pi}{2}}\cdot\sin c\left[(k_{m_1}-k_x)\frac{a}{2}\right]\right] \tag{15}$$

$$\tilde{I}_{ym}=\frac{ib}{2}\left[e^{-i\frac{m_2\pi}{2}}\cdot\sin c\left[(k_{m_2}+k_y)\frac{b}{2}\right]-e^{i\frac{m_2\pi}{2}}\cdot\sin c\left[(k_{m_2}-k_y)\frac{b}{2}\right]\right] \tag{16}$$

2.3.2. Sinusoidal Basis Function with Edge Conditions (sbf-w-ec)

The components of the current density $J_{xn}(r_S)$ and $J_{ym}(r_S)$ present end-point singularities due to the terms contained in their respective denominators.

It is usual to expand the unknown functions as follows

$$J_{xn}(\mathbf{r}_s) = \sin\left[\frac{n_1\pi}{a}\left(x+\frac{a}{2}\right)\right]\cdot\frac{\cos\left[\frac{n_2\pi}{b}\left(y+\frac{b}{2}\right)\right]}{\sqrt{1-\left(\frac{2y}{b}\right)^2}} \tag{17}$$

$$J_{ym}(\mathbf{r}_s) = \frac{\cos\left[\frac{m_1\pi}{a}\left(x+\frac{a}{2}\right)\right]}{\sqrt{1-\left(\frac{2x}{a}\right)^2}}\cdot\sin\left[\frac{m_2\pi}{b}\left(y+\frac{b}{2}\right)\right] \tag{18}$$

The scalar Fourier transform of each equation is given by

$$\tilde{\mathbf{J}}_{xn}(\mathbf{k_s})=\tilde{I}_{xn}\cdot\tilde{I}_{xm} \qquad \tilde{\mathbf{J}}_{ym}(\mathbf{k_s})=\tilde{I}_{yn}\cdot\tilde{I}_{ym} \tag{19}$$

where,

$$\tilde{I}_{xn} = \frac{ia}{2}\left[e^{-i\frac{n_1\pi}{2}}\cdot\sin c\left[(k_{n_1}+k_x)\frac{a}{2}\right] - e^{i\frac{n_1\pi}{2}}\cdot\sin c\left[(k_{n_1}-k_x)\frac{a}{2}\right]\right] \quad (20)$$

$$\tilde{I}_{xm} = \frac{b\pi}{4}(-i)^n\left[J_0\left(\frac{k_y b}{2}-\frac{n_2\pi}{2}\right)+(-1)^n J_0\left(\frac{k_y b}{2}+\frac{n_2\pi}{2}\right)\right] \quad (21)$$

$$\tilde{I}_{yn} = \frac{\pi a}{4}(-i)^n\left[J_0\left(\frac{k_x a}{2}-\frac{m_1\pi}{2}\right)+(-1)^n J_0\left(\frac{k_x a}{2}+\frac{m_1\pi}{2}\right)\right] \quad (22)$$

$$\tilde{I}_{ym} = \frac{ib}{2}\left[e^{-i\frac{m_2\pi}{2}}\cdot\sin c\left[(k_{m_2}+k_y)\frac{b}{2}\right] - e^{i\frac{m_2\pi}{2}}\cdot\sin c\left[(k_{m_2}-k_y)\frac{b}{2}\right]\right] \quad (23)$$

J_0 is the zeroth-order Bessel function.

2.3.3. Chebyshev Polynomials with Edge Conditions (cp-ec)

In this set, the current density forms are given by the following expressions

$$J_{xn}(\mathbf{r}_s) = \left[\sqrt{1-(2x/a)^2}U_{n_1}\left(\frac{2x}{a}\right)\right]\left[\frac{T_{n_2}(2y/b)}{\sqrt{1-(2y/b)^2}}\right] \quad (24)$$

$$J_{ym}(\mathbf{r}_s) = \left[\frac{T_{m_1}(2x/a)}{\sqrt{1-(2x/a)^2}}\right]\left[\sqrt{1-(2y/b)^2}U_{m_2}\left(\frac{2y}{b}\right)\right] \quad (25)$$

where $T\cdot$ and $U\cdot$ are, respectively, the first and second kinds of Chebyshev's polynomials. The Fourier transforms of (24) and (25) are given by

$$\tilde{J}_{xn}(\mathbf{k_s}) = \pi^2\frac{ab}{8}(-i)^{n_1+n_2}\left[J_{n_1}\left(k_x\frac{a}{2}\right)+J_{n_1+2}\left(k_x\frac{a}{2}\right)\right]\left[J_{n_2}\left(k_y\frac{b}{2}\right)\right] \quad (26)$$

$$\tilde{J}_{ym}(\mathbf{k_s}) = \pi^2\frac{ab}{8}(-i)^{m_1+m_2}\left[J_{m_2}\left(k_y\frac{b}{2}\right)+J_{m_2+2}\left(k_y\frac{b}{2}\right)\right]\left[J_{m_1}\left(k_x\frac{a}{2}\right)\right] \quad (27)$$

The analytic model of concern, taking into account preceding modal decomposition, allows to determine the resonant frequency for selected RPRs' dimensions for different substrate and superstrate materials.

3. NUMERICAL RESULTS

3.1. Convergence and Computing Time

The convergence and computing time are among the most important criteria leading to the efficiency of a numerical approach. The obtained

resonant frequency of a single layer structure for different types and numbers of basis functions is presented in Table 1.

The rectangular microstrip patch considered here is of dimensions $a = 25\,\text{mm}$ and $b = 15.357\,\text{mm}$ implemented on a substrate with relative permittivity of 2.2. The dimensions of substrate are $W_1 = 50\,\text{mm}$, $L_1 = 40\,\text{mm}$ and $d_1 = 0.8\,\text{mm}$.

The codes have been developed with the Fortran 90 language running on a PC equipped with INTEL® CORE™ 2 DUO, 3.0 GHz Processor and 2.0 Gigabyte RAM. For a single layer microstrip patch, the calculation time of the resonant frequency is on the average around 148 s for CST, 124 s for HFSS, 343 s for sbf-wo-ec, 794 s for sbf-w-ec and 321 s for cp-ec.

The S-parameters convergence criterion has been reached after calculating 9 frequency samples for CST and cp_ec, 11 frequency samples for HFSS and sbf_w_ec and 27 frequency samples for sbf_wo_ec.

It can be noticed that an excellent convergence of the resonant frequency is obtained with a truncation of the improper infinite double integrals given by Equations (5a)–(5e), at $k_s = 60k_0$ for the sbf-wo-ec, $50k_0$ for the sbf-w-ec and $30k_0$ for the cp-ec [14].

We observe that the proposed model reaches convergence using

Table 1. Resonant frequency with different types and numbers of basis functions vs substrate thickness, for a single layer RPR; d_1 is measured in mm.

Types of basis functions	**Number of basis functions**		**Frequency (GHz)**						
			d_1**=0.8**	d_1**=1**	d_1**=1.6**	d_1**=2**	d_1**=2.5**	d_1**=3**	d_1**=3.5**
	N =1	M=1	5.295	5.182	4.925	4.786	4.651	4.522	4.408
sbf-wo-ec	N =3	M=2	5.295	5.182	4.925	4.786	4.651	4.522	4.408
	N =3	M=3	5.292	5.180	4.924	4.788	4.650	4.523	4.414
	N =1	M=1	6.110	6.067	5.895	5.753	5.623	5.489	5.360
sbf-w-ec	N =3	M=2	6.110	6.067	5.895	5.753	5.623	5.489	5.361
	N =3	M=3	6.100	6.067	5.889	5.751	5.623	5.489	5.361
	N =1	M=1	6.333	6.255	6.123	6.009	5.889	5.779	5.665
cp-ec	N =3	M=2	6.333	6.255	6.123	6.009	5.889	5.779	5.665
	N =3	M=3	6.392	6.257	6.125	6.003	5.892	5.751	5.667

only two basis functions ($N = 1$ and $M = 1$). Nevertheless, we have worked a number of basis functions equal to 6 ($N = 3$ and $M = 3$).

The convergent resonant frequencies for different substrate thicknesses are in an excellent agreement with the EM simulation data and experiment results (Table 1).

A similar study on the convergence and CPU time were made on a RPR with superstrate (Figure 1). The same rectangular patch of the previous case is inserted between two isotropic dielectrics (Duroid permittivity $\varepsilon_r = 2.2$ and $\mathrm{tg}\delta = 9 \times 10^{-4}$); the planar dimensions of the isotropic substrate and superstrate are the same ($W_{1,2} = 50\,\mathrm{mm}$, $L_{1,2} = 40\,\mathrm{mm}$). The substrate and superstrate thicknesses are $d_1 = d_2 = 0.8\,\mathrm{mm}$. We notice that the convergence is also reached using only two basis functions but with a greater CPU time than the one obtained for the single layer structure.

The use of various current expansion functions, based on physical considerations fulfilling the boundary conditions on the patch, yields the following conclusions

1) Based on some physical considerations and developed using the cavity model theory, the sbf-wo-ec, used to expand the unknown currents on the patch, is easy to formulate theoretically. However, a slow convergence in the MoM solution should be expected.
2) Due to their weighting factors representing true boundary conditions, the sbf-w-ec give a good approximation of the unknown functions. Additionally, faster convergence than the first type of functions is observed. Moreover, their Fourier transforms involve tedious manipulations in which special Bessel functions are ineluctable.
3) The cp-ec involves the use of Bessel functions of higher order, yielding complex numerical implementation and theoretical formulation, but a faster numerical convergence.

3.2. Comparison Between Proposed Model and Existing Results

As a validation of the different results, we have compared the proposed model (with and without superstrate, anisotropic and isotropic layers) with published experimental data.

The measurement of the precision criterion is defined as the relative shift of the simulated (or measured) frequency versus the appropriated reference frequency.

The formula is given by

$$\Delta f_r / f_r(\%) = [|f_{\mathrm{ref}} - f_{r\,\mathrm{simulation}|}/f_{\mathrm{ref}}] * 100 \tag{28}$$

Table 2. Comparison of the calculated resonant frequency with measured and calculated data [15], for a single anisotropic layer; $d_2 = 0$, $\varepsilon_{rx} = 13.0\,(\text{tg}\delta = 0)$, $\varepsilon_{rz} = 10.0\,(\text{tg}\delta = 3.5 \times 10^{-3})$.

d_1 (mm)	a (mm)	b (mm)	Resonance Frequency (GHz)					$\Delta f_r/f_r(\%)$		
			Meas. [15]	Calc. [15]	Sbf wo-ec	Sbf w-ec	cp-ec	Sbf wo-ec	Sbf w-ec	cp-ec
1.27	20.0	30.0	2.264	2.268	2.261	2.263	2.268	0.1	0.1	0.2
1.27	9.5	15.0	4.495	4.520	4.355	4.419	4.369	3.0	1.7	3.0
2.54	19.0	30.0	2.242	2.260	2.177	2.209	2.181	2.9	1.5	2.7

where, f_{ref} is the measured frequency [15].

The resonant frequency of the RPR presented in Figure 1 without superstrate ($d_2 = 0$) is calculated and compared with the results presented in [15]. Table 2 illustrates two types of anisotropic structures ($\varepsilon_{rx} = 13.0$, $\varepsilon_{rz} = 10.0$). The first one represents two different substrate thicknesses while the second represents different patch dimensions.

As can be seen from Table 2, a good agreement is observed between our calculated data and results reported in [15]. The resonant frequency relative error ($\Delta f_r/f_r$) gives an average value less than 2%, showing again the accuracy of our results.

A similar comparison was also done for two RPRs having the same dimensions, except that their substrate was considered as isotropic with different values of permittivity ($\varepsilon_{rx} = \varepsilon_{rz} = 13.0$ or $\varepsilon_{rx} = \varepsilon_{rz} = 10.0$). The agreement between our results and those of [15] can be quantified by the average of the resonant frequency shift error, less than 14% for a structure with isotropic substrate ($\varepsilon_{rx} = \varepsilon_{rz} = 13.0$) and less than 5% for a structure with isotropic substrate ($\varepsilon_{rx} = \varepsilon_{rz} = 10.0$).

3.3. Model Validation with Commercial Software Algorithms

While the effect of the isotropic substrate thickness on the resonant frequency is shown in Figures 2(a), 2(b) with and without superstrate, respectively, the effect of the isotropic superstrate thickness on the resonant frequency is shown in Figure 2(c).

The rectangular patch ($a = 25\,\text{mm}$ and $b = 15.357\,\text{mm}$) is inserted between two isotropic dielectrics (Duroid permittivity $\varepsilon_r = 2.2$ and $\text{tg}\delta = 9 \times 10^{-4}$); the planar dimensions of the isotropic substrate

and superstrate are the same ($W_{1,2} = 50\,\text{mm}$, $L_{1,2} = 40\,\text{mm}$). In Figures 2(a), 2(b), the superstrate thickness is constant ($d_2 = 0.8\,\text{mm}$), and the substrate thickness d_1 varies. In Figure 2(c) the substrate thickness is constant ($d_1 = 0.8\,\text{mm}$), and the superstrate thickness d_2 varies.

First of all, a comparison of the curves resonant frequency versus d_1 (Figures 2(a), 2(b)) shows the effect of the superstrate on the resonant frequency.

On the other hand, a glance at Figure 2 shows a qualitative agreement with published data [12–16].

Figures 2(a), 2(b) show the effect of the thickness substrate on the

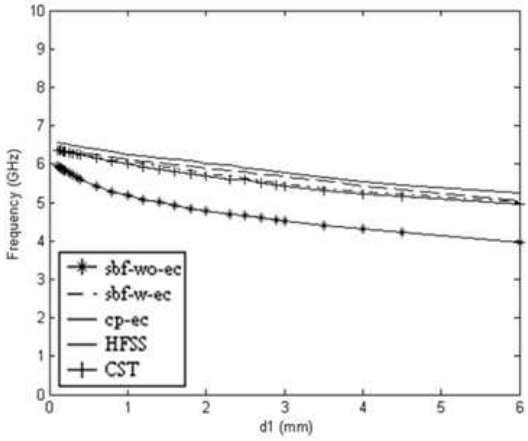

(a)

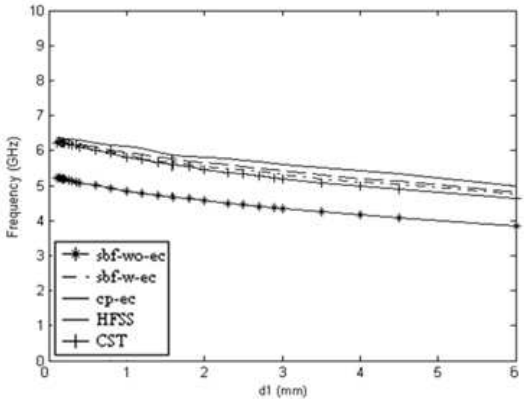

(b)

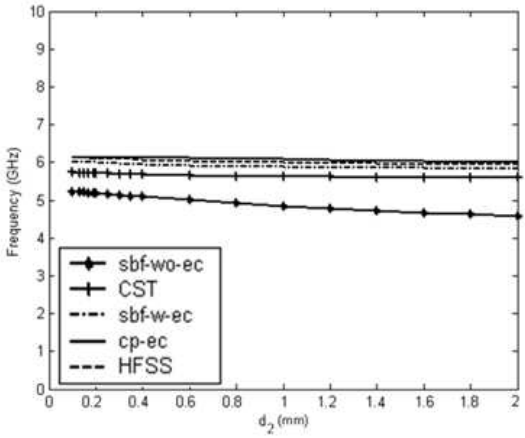

(c)

Figure 2. (a) Resonant frequency without superstrate versus d_1, for $d_2 = 0$. (b) Resonant frequency with superstrate versus d_1, for $d_2 = 0.8\,\text{mm}$. (c) Resonant frequency versus d_2, for $d_1 = 0.8\,\text{mm}$.

resonant frequency. We observe that the values of resonant frequency with superstrate are slightly lower than those obtained from a single layer structure. This is primarily due to the effective permittivity of the region under the patch. As the substrate gets thicker, similar values of the resonant frequency are obtained. However, when the substrate thickness gets lower and mainly when $d_1 < d_2$, the effect of the substrate decreases, and the resonant frequency becomes mainly related to the superstrate. Consequently, the obtained results are in a perfect concordance with the literature [2].

As for the comparison of the proposed model with HFSS and CST, we remark that there is a good agreement between HFSS and CST with sbf-w-ec and cp-ec. However, the sbf-wo-ec model gives a similar behavior with a considerable gap. This can be attributed to the absence of edge singularities. For this reason, it is not considered in the subsequent sections.

In Figure 2(c), we consider the effect of d_2 on the resonant frequency. Here also, we notice that similar curve behaviors are obtained for HFSS, CST, sbf-wo-ec, sbf-w-ec and cp-ec. Nevertheless, when the superstrate is thicker, the constant resonant frequency becomes 4.5 GHz for sbf_wo_ec, 5.6 GHz for sbf_w_ec, 6.4 GHz for cp_ec, and 5.9 GHz for HFSS and 5.8 GHz for CST.

4. RPR PROTOTYPE FABRICATION AND MEASUREMENTS

Initially, four RPRs prototypes with two thicknesses with and without superstrate were designed and simulated then fabricated and measured. Afterwards, the measured dimensions values have been reinserted in the commercial simulators in order to minimize the shift between the simulated data and the measurements. The standard deviations in the RPRs parameters were taken into account to estimate accuracy of resonant frequency.

4.1. Experimental Setup

Several structures of RPR have been realized on the Rogers RT/Duroid 5880^{TM} permittivity given by the datasheet 2.2 ± 0.02, tg$\delta = 9 \times 10^{-4}$ for 1–10 GHz [17].

The actual dimensions of RPR structures which were measured after fabrication were taken into account. The two resonators were defined as follows.

The first resonator (RPR-1) without superstrate ($d_2 = 0$) and rectangular patch dimensions $a = 25 \pm 0.08$ mm and $b = 15.357 \pm 0.08$ mm, is printed on a Duroid isotropic substrate, with dimensions $W_1 = 50$ mm, $L_1 = 40$ mm. The dispersion on W_1 and L_1 are, respectively, ± 2 mm and ± 1 mm, and the substrate thicknesses are $d_1 = 0.8 \pm 0.04$ mm and 1.6 ± 0.04 mm.

The second resonator (RPR-2) is similar to the first one but with the presence of the superstrate of dimensions $W_2 = 50$ mm, $L_2 = 40$ mm. The dispersions on W_2 and L_2 are, respectively, ± 2 mm and ± 1 mm, and the thickness is constant ($d_2 = 0.8 \pm 0.04$ mm).

The measurements of the resonant frequency were made with a vectorial network analyzer (VNA-ANRITSU MS 2028 B) at room temperature 25°C. The SOLT calibration was performed on the frequency band 1–12 GHz. The results are shown in Figures 3(a) and 3(b). The fundamental resonance mode and several other superior modes are observed.

4.2. Experimental Results of the RPRS with Substrate and Superstrate

RPR prototypes have been realized with different substrate permittivities (in this paper we take only Duroid structure) and thicknesses, with and without superstrate. In order to quantify real physical dimensions dispersion effects of the RPRs, all their dimensions have been carefully measured.

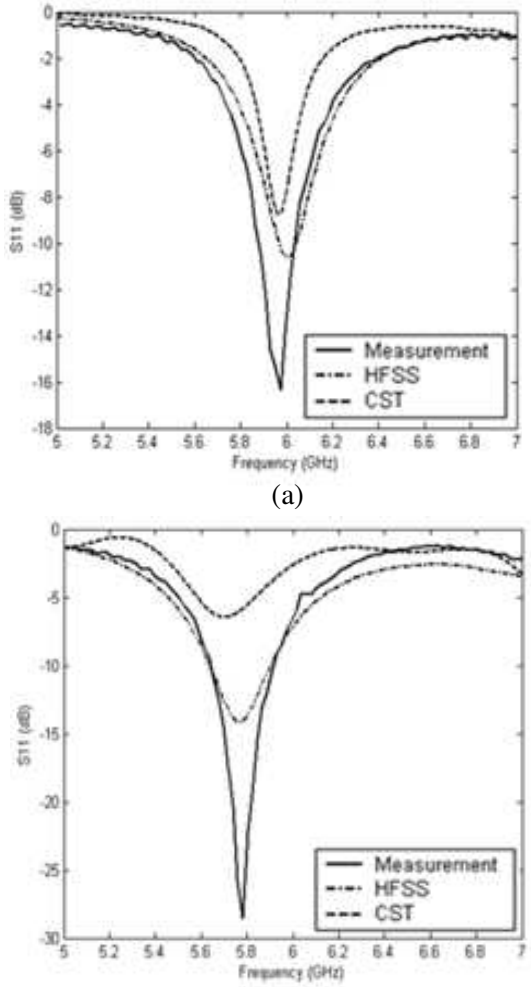

Figure 3. Measurement and simulation with HFSS and CST results for substrate thickness (a) $d_1 = 0.84\,\text{mm}$ of RPR-2, (b) $d_1 = 1.64\,\text{mm}$ of RPR-2.

As an example, two cases are studied. The first case consists of a rectangular patch resonator ($a = 25.08\,\text{mm}$ and $b = 15.438\,\text{mm}$) inserted between two similar isotropic dielectrics as substrate and superstrate (Duroid permittivity $\varepsilon_r = 2.2$ and $\text{tg}\delta = 9 \times 10^{-4}$), with a similar dimension ($W_{1,2} = 52\,\text{mm}$, $L_{1,2} = 41\,\text{mm}$). The substrate and superstrate thicknesses are constant, given, respectively,

Table 3. Comparison of calculated resonant frequency through HFSS and CST simulations, proposed data model and VNA measurements, for a single isotropic layer; Duroid substrate $\varepsilon_r = 2.2$, $d_1 = 0.84$ and 1.64 mm, $d_2 = 0$ mm.

d_1	Frequency (GHz)					$\Delta f_r/f_r(\%)$			
(mm)	Measurements	sbf w-ec	cp-ec	HFSS	CST	sbf w-ec	cp-ec	HFSS	CST
0. 84	6.057	6.092	6.309	6.150	6.158	0. 6	4.2	1.5	1.7
1.64	5.887	5.883	6.114	6.010	5.890	0.1	3.9	2.1	0.1

Table 4. Comparison of calculated resonant frequency through HFSS and CST simulations, proposed data model and VNA measurements, for a two isotropic layer; Duroid substrate $\varepsilon_{rx} = \varepsilon_{rz} = 2.2$, $d_1 = 0.84$ and 1.64 mm and Duroid superstrate $\varepsilon_r = 2.2$, $d_2 = 0.84$ mm.

d_1	Frequency (GHz)					$\Delta f_r/f_r(\%)$			
(mm)	Measurements	sbf w-ec	cp-ec	HFSS	CST	sbf w-ec	cp-ec	HFSS	CST
0. 84	5.972	5.977	6.162	6.00	5.968	0.1	3.2	0.5	0.1
1.64	5.781	5.757	5.833	5.77	5.722	0.4	0.9	0.2	1.0

as $d_1 = 0.84$ mm and $d_2 = 0.84$ mm. In the second case, the same resonator is used with substrate thickness $d_1 = 1.64$ mm.

Figures 3(a) and 3(b) show measurement and simulation results of the return loss versus frequency of RPR-2 (with superstrate and two substrate thicknesses). Our concern was only with the dominant fundamental mode around 6 GHz.

The results given by simulations through HFSS and CST and our measurements were similar. The small difference resides in the meshing or simulation step.

The measured fundamental frequency of this RPR is taken as the reference frequency (Equation (28)).

The agreement between these results can be quantified by the average of the resonant frequency relative error $\Delta f_r/f_r$, evaluated as 1.9% with HFSS and 0.9% with CST for the resonator without superstrate (Table 3) and 0.5% with HFSS and 2% with CST for the resonator with superstrate (Table 4).

4.3. Discussion

Tables 3 and 4 summarize the proposed data model, simulations (HFSS and CST) and VNA measurements established from Figures 2 and 3. The relative error $\Delta f_r/f_r$ is determined for all RPR configurations under investigation.

According to these tables, the sbf-w-ec gives a better approach than the real form of the unknown functions. The values are almost similar to those obtained by simulation. The relative error averages for a substrate thickness $d_1 = 0.84\,\text{mm}$ are 2% (without superstrate) and 1% (with superstrate),

Considering the results obtained for substrate thickness $d_1 = 1.64\,\text{mm}$, we have obtained average values of the relative error as 1.5% without superstrate and 0.6% with superstrate.

Geometrical parameters effects of substrate and superstrate thicknesses on resonant frequency shift are discussed, and the dispersion results due to the real physical dimensions of the resonators were taken into account.

For measurements, we used a Vectorial Network Analyzer (Anritsu) with maximum number points of 1601 in the frequency range of interest. For the sweep frequency range (12 GHz), the frequency step between two near measures is about 7 MHz, giving then the frequency resolution. RPR measurements were repeated for the same configurations and showed a very good reproducibility.

4.4. Comparison with Dielectric Relative Permittivity Tolerance

The permittivity accuracy of the Rogers RT/Duroid 5880$^{\text{TM}}$ given by the datasheet (2.2 ± 0.02, $\text{tg}\delta = 9 \times 10^{-4}$ for a frequency band 1–10 GHz) [17] was also taken into consideration. HFSS and CST simulations with three values of the permittivity $\varepsilon_r = 2.18, 2.2$ and 2.22 were treated for RPR with and without superstrate (see dimensions in Subsection 4.1). The obtained relative errors in Table 5 are given only for thicknesses $d_{1,2} = 0.84\,\text{mm}$.

In this table, the relative error is calculated using our measured reference values (5.972 GHz for the RPR with superstrate and 6.057 GHz for the RPR without superstrate). We may notice qualitative agreement and accuracy with average relative errors of 0.1% with superstrate and 2% without superstrate. Also, the tolerance of the permittivity may lead to a relative error on the resonant frequency of the same range.

Since the influence of the superstrate on the resonator performance was considered, the numerical results indicate that the real part of

Table 5. Effect of relative permittivity tolerance on resonant frequency, for the RPR with and without superstrate; thicknesses $d_1 = d_2 = 0.84\,\text{mm}$.

ε_r	$\Delta f_r/f_r(\%)$			
	Without superstrate		With superstrate	
	CST	HFSS	CST	HFSS
2.18	2.0	1.9	0.3	0.8
2.2	1.7	1.5	0.1	0.5
2.22	1.0	1.0	0.7	0.1

the resonant frequency of the structures with dielectric superstrate is slightly smaller than that of the single layer structure. This is due to the effective permittivity of the environment surrounding the conductive patch, which increases more in RPR-1 than in RPR-2.

The effect of the superstrate becomes perceptible as its thickness increases. We observe that the resonant frequency of the structures with superstrate tends to decrease with respect to the single layer structures due to the effect of the edge field and the EM radiation which are more important in RPR-1 than in RPR-2.

5. CONCLUSION

In this paper, RPRs, with and without superstrate, have been designed and experimentally measured. The resonant frequency has been treated subject to the effects of various parameters such as substrate and superstrate thicknesses, patch dimensions, permittivity. Then accuracy of the obtained results has been investigated. A comparative study of our proposed model results, published works, simulations with EM commercial software algorithms HFSS and CST and VNA measurements on some prototypes has been conducted. Fast numerical convergence has been reached using only two entire-domain sinusoidal basis functions. In all cases, we obtained very good agreements between our results and the one found in the literature. In general, a good accuracy on the dominant resonant frequency is observed with an average error less than 2% among the proposed model results, simulation and measurements results. The proposed model introducing basis functions and taking into account edge singularities corresponds to a good approach to the cavity model, particularly, the sinusoidal basis function with edge conditions appearing to be a better approximation than our experimental results (about 0.3%).

REFERENCES

1. Pozar, D. M., *Microwave Engineering*, Addison-Wesley, New-York, 1990.
2. Bouttout, F., F. Benabdelaziz, T. Fortaki, and D. Khedrouche, "Resonant frequency and bandwidth of a superstrate-loaded rectangular patch on a uniaxial anisotropic substrate," *Communications in Numerical Methods in Engineering*, Vol. 16, No. 7, 459–473, John Wiley & Sons, Jul. 2000.
3. Newman, E. H. and D. Forrai, "Scattering from a microstrip patch," *IEEE Trans. Antennas Propagat.*, Vol. 35, 245–251, Mar. 1987.
4. Tounsi, M. L., R. Touhami, and M. C. E. Yagoub, "Dynamic analysis of multilayered anisotropic finline and microstrip resonators," *Journal of Microwave and Optoelectronics*, Vol. 5, No. 2, 88–100, Dec. 2006.
5. Essid, C., M. B. B. Salah, K. Kochlef, A. Samet, and A. B. Kouki, "Spatial-spectral formulation of method of moment for rigorous analysis of microstrip structures," *Progress In Electromagnetics Research Letters*, Vol. 6, 17–26, 2009.
6. Hassani, H. R. and M. Jahanbakht, "Method of moment analysis of finite phased array of aperture coupled circular microstrip patch antennas," *Progress In Electromagnetics Research B*, Vol. 4, 197–210, 2008.
7. Mittra, R. and K. Du, "Characteristic basis function method for iteration-free solution of large method of moments problems," *Progress In Electromagnetics Research B*, Vol. 6, 307–336, 2008.
8. See, K. Y., E. K. Chua, and Z. H. Liu, "Accurate and efficient evaluation of MoM matrix based on a generalized analytical approach," *Progress In Electromagnetics Research*, Vol. 94, 367–382, 2009.
9. Mathis, A. W. and A. F. Peterson, "Efficient electromagnetic analysis of a doubly infinite array of rectangular apertures," *IEEE Trans. Microwave Theory Tech.*, Vol. 46, 46–54, Jan. 1998.
10. Wong, K. L., J. S. Row, C. W. Kuo, and K. C. Huang, "Resonance of a rectangular microstrip patch on a uniaxial substrate," *IEEE Trans. Microwave Theory Tech.*, Vol. 41, No. 4, 698–701, Apr. 1993.
11. Row, J. S. and K. L. Wong, "Resonance in a superstrate-loaded rectangular microstrip structure," *IEEE Trans. Microwave Theory Tech.*, Vol. 41, No. 8, 1349–1354, Aug. 1993.
12. Chew, W. C. and Q. Liu, "Resonance frequency of a rectangular

microstrip patch," *IEEE Trans. Antennas Propagat.*, Vol. 36, 1045–1056, Aug. 1988.

13. Aouabdia, N., F. Benabdelaziz, F. Bouttout, and H. Baudrand, "Etude spectrale d'une antenne microbande piégée de forme rectangulaire selon trios types de modélisation du courant de conduction. Application au gap d'air," *XVII^{ème} Colloque International, Optique Hertzienne et Diélectrique (OHD 2003)*, Calais-France, Sep. 3–5, 2003.
14. Aouabdia, N., F. Benabdelaziz, F. Bouttout, C. Zebiri, and F. Benmeddour, "Resonant frequency of rectangular microstrip antenna depends of the dielectric substrate parameters using the various types of currents expansion function," *IEEE Proceeding, First International Symposium on Control, Communications and Signal Processing (ISCCSP)*, 347–350, Tunisia, Mar. 21–24, 2004.
15. Pozar, D. M., "Radiation and scattering from a microstrip patch on a uniaxial substrate," *IEEE Trans. Antennas Propagat.*, Vol. 35, 613–621, Jun. 1987.
16. Chew, W. C. and Q. Liu, "Correction to resonance frequency of a rectangular microstrip patch," *IEEE Trans. Antennas Propagat.*, Vol. 36, 1827, Dec. 1988.
17. Data sheet RT/Duroid 5870/5880 Laminates, Advanced Circuit Materials Division, www.rogerscorp.com, Rogers Corporation.